

Effect of bonding duration and substrate temperature in copper ball bonding on aluminium pads: A TEM study of interfacial evolution

H. Xu^{a,*}, C. Liu^a, V.V. Silberschmidt^a, Z. Chen^b, J. Wei^c, M. Sivakumar^d

^a Wolfson School of Mechanical and Manufacturing Engineering, Loughborough University, Loughborough, LE11 3TU, UK

^b School of Materials Science and Engineering, Nanyang Technological University, Nanyang Avenue, Singapore 639798, Singapore

^c Singapore Institute of Manufacturing Technology, 71 Nanyang Drive, Singapore 638075, Singapore

^d ASM Technology Singapore, 2 Yishun Avenue 7, Singapore 768924, Singapore

ARTICLE INFO

Article history:

Received 31 January 2010

Received in revised form 24 March 2010

Accepted 24 March 2010

Available online 15 May 2010

ABSTRACT

The effect of bonding duration and substrate temperature on the nano-scale interfacial structure for bonding strength were investigated using high resolution transmission electron microscopy. It shows that intermetallic compound crystallization correlates with bonding duration, as a longer duration is applied, alumina fragmentation becomes pervasive, resulting in continuous alloy interfaces and robust bonds. In addition, a substrate temperature (i.e. 175 °C) promotes the fracture of alumina, and simultaneously contributes to the interfacial temperature, accelerating interdiffusion and facilitating the formation of intermetallic compounds, therefore increasing bonding strength. The compound formed during bonding is CuAl₂, regardless of the bonding parameters applied.

© 2010 Elsevier Ltd. All rights reserved.

1. Introduction

There is growing interest in Cu wire bonding for fine pitch application due to cost saving and better mechanical and electrical properties. In this process, a thin copper wire is bonded to an aluminium metallization pad using a combination of ultrasonic energy, pressure (~150 MPa) and heat (150–220 °C). It is a complex process, and the physics has not been fully understood. However, many efforts have been made to study and explain the process [1–16]. In general, three experimental approaches have been used to investigate the mechanisms of the bond formation. The first one concentrates on experimentally *in situ* measurements of interfacial temperature during bonding [1–3]. The second one considers an explanation of characteristics of the observed footprints on the bond pads or the bottom of bonds [4–9]. The third one is based on the cross-sectional characterization of the interfacial microstructure in wire bonds [10–12]. The main proposed theories include melting [13], fretting [14] and micro-slip [15,16]. Melting was postulated that ultrasonic vibration caused rubbing between a wire and a pad, resulting in significant increase of the interfacial temperature, so melting took place in local areas, leading to bonding [13]. However, there are a quantity of experimental evidences to show that although there is a temperature rise, it does not approach the melting point of the materials. For example, the highest measured interfacial temperature during bonding by far is 320 °C [3], and it is far below the melting point of bonding

materials (Al 660 °C, Au 1063 °C and Cu 1083 °C). In addition, bonding was successfully performed in liquid nitrogen at 77 K and without any bubbles being observed, implying that temperature rise is not a must for bonding [1,17]. Furthermore, a TEM examination of the bond interface indicated no evidence of melting [18]. The fretting theory was proposed by Hulst and Lasance [14] who argued that interfacial sliding between a wire and a pad cleaning and heating surface is a key for bonding. However, a measurement of the movement of the wire during bonding using a laser interferometer by Wilson [19] showed that the wire position remained fixed relative to the substrate during bonding, although the capillary tool moved with an amplitude of 0.5–2.5 μm, so bonding can be successful even when there is no interfacial motion. In addition, the sliding model predicted preferential bonding at the centre of the interface; however it was reported that bonding initiated near the periphery [4,20]. Chen [15] introduced Mindlin's micro-slip theory [16] to explain the interfacial characteristics of wire bonds. In the proposed model, the central contact region was termed an elastic or non-slip region, while the outer contact area was represented as an exhibiting slip, termed a micro-slip. This fits the commonly observed pattern of the bonds where bonding predominated at the edge of the contact area rather than at the centre. All those mechanisms assume that removal of a ubiquitous native alumina overlayer is essential for successful bonding as it acts as a barrier to diffusion, and recently, this has been verified experimentally in our previous work by high resolution transmission electron microscopy (HRTEM) [10]. It showed that the ultrasonic vibration under certain pressure and heat partially fragments the native alumina layer (~10 nm thick), providing the

* Corresponding author. Tel.: +44 (0) 1509 227684.

E-mail addresses: H.Xu3@lboro.ac.uk, huixu.hit@gmail.com (H. Xu).

pathways for Cu–Al interdiffusion. This promotes formation of the intermetallic compounds (IMCs) and consequently improves the bonding strength significantly. On the other hand, the influence of bonding parameters – ultrasonic power, bonding force, bonding duration and substrate temperature – on bonding strength were well documented [8,21–23]. Nonetheless, a full account of the underlying mechanistic aspects has not been presented, since there were few reports on interfacial structural changes due to variation of bonding parameters.

In this paper, the effects of bonding duration and substrate temperature on the behaviour of the interfacial microstructure (alumina, IMCs, defects, etc.) was investigated using dual beam focused ion beam (FIB) and HRTEM. A relationship between those parameters, interfacial structure and bonding strength is established.

2. Experimental methods

Thermosonic copper ball bonding was conducted with an ASM Eagle 60AP ball/wedge automatic bonder. The copper wire (99.99 wt.%) was 20 μm in diameter with a break strength of 4.3–9.2 gf (1 gf = 9.8 mN) and an elongation of 5–15%. The aluminium pad is 1 μm thick on SiO_2/Si . An electrical flame off (EFO) process with a 48 mA current, 4500 V gap voltage and 290 μs discharge time produced a free air ball (FAB) at the copper wire tip. Specifically, a shielding gas (95% N_2 –5% H_2) with the gas flow rate of 0.6 l/min was utilized to prevent the oxidation of copper during EFO ball formation. After cooling, the copper ball was transferred onto the bond pad to form the Cu/Al bond using a combination of a normal force, transverse ultrasonic vibration and heat. Three bonding duration settings (levels BT1, BT2 and BT3) (Table 1) and three substrate temperature settings (ST1, ST2 and ST3) (Table 2) were selected so that their effects on the interfacial structure and bonding strength could be

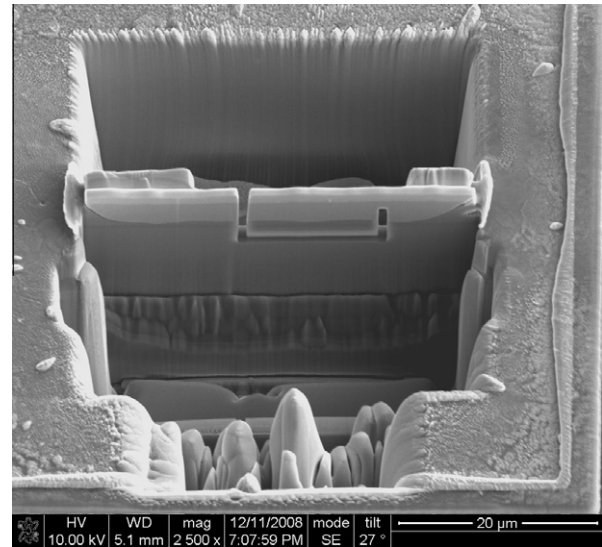


Fig. 1. Region-specific TEM sample preparation using FIB.

studied. To reduce post-thermal effects on interfacial characteristics, the bonded samples were removed immediately from the work stage, but inevitably maintained at substrate temperature for ~ 5 s.

Cross-sections of the Cu/Al bonds were prepared by FIB for scanning electron microscopy (SEM) and transmission electron microscopy (TEM) analysis. All TEM samples were selected from the central regions of the interface, an example of which is shown in Fig. 1. The nanostructure at the interface, including alumina and IMCs, were investigated by TEM combined with energy dispersive X-ray spectrometry (EDX). TEM analysis was carried out using a

Table 1
Bonding parameters for three levels of bonding duration^a.

Bonding parameters	Level-BT1 (short duration)	Level-BT2 (standard)	Level-BT3 (long duration)
Standby power ^b , DAC	12 (210.0 nm) ^c	12 (210.0 nm)	12 (210.0 nm)
Contact power, DAC ^d	10 (175.0 nm)	10 (175.0 nm)	10 (175.0 nm)
Contact force, mN	220	220	220
Contact duration, s	0.001	0.003	0.005
Bonding power, DAC	36 (630.0 nm)	36 (630.0 nm)	36 (630.0 nm)
Bonding force, mN	180	180	180
Bonding duration, s	0.002	0.006	0.010
Substrate temperature, °C	175	175	175

^a A whole bonding duration consists of two basic stages: (i) contact stage and (ii) bonding stage. During the contact stage, a high bonding force and a low ultrasonic power are usually employed to cause big plastic deformation of the balls; during the bonding stage, a low bonding force and a high ultrasonic power are used to ensure robust bonds. Interdiffusion and IMC formation take place during the latter stage, so the bond strength is mainly determined by the bonding stage.

^b Standby power is ultrasonic power used before the contact stage.

^c Ultrasonic amplitudes of the capillary tip are listed in brackets.

^d DAC is an ASM internal energy unit. It is the abbreviation of digital to analog conversion.

Table 2
Bonding parameters for three levels of substrate temperature.

Bonding parameters	Level-ST1 (room temperature)	Level-ST2 (standard, 175 °C)	Level-ST3 (300 °C)
Standby power, DAC	12 (210.0 nm)	12 (210.0 nm)	12 (210.0 nm)
Contact power, DAC	10 (175.0 nm)	10 (175.0 nm)	10 (175.0 nm)
Contact force, mN	220	220	220
Contact duration, s	0.003	0.003	0.003
Bonding power, DAC	36 (630.0 nm)	36 (630.0 nm)	36 (630.0 nm)
Bonding force, mN	180	180	180
Bonding duration, s	0.006	0.006	0.006
Substrate temperature, °C	25	175	300

JEOL 2100F system at 200 kV. A microprobe beam (0.7 nm diameter) was used for composition analysis with EDX in scanning (S)TEM mode. Fast Fourier transformation (FFT) of lattice images calculated using ImageJ 1.42q [24] was utilized to identify Cu–Al IMCs.

The shear tests were conducted with a DAGE 4000 micro-tester at a tool height of 3 μm and a tool movement speed of 4 μm/s. To avoid the effect of squeezed Al pad on bonding force, the shear tests were performed to the vertical direction of the ultrasonic vibration during wire bonding. The load that causes the fracture of the bonds is termed shear force. The shear strength was obtained as pressure, i.e. shear force per unit area. The dimension of the bonds were defined by two parameters – ball diameter *D* and ball height *H*. $D = (D_A + D_B)/2$, where D_A and D_B are the diameters of the mashed ball along and vertical to the direction of the ultrasonic vibration, respectively. The ball diameter is usually used to roughly represent the bonding area. The ball height *H* is the distance between the top surface of the bond pad and the edge of the mashed ball. The values of D_A , D_B and *H* were recorded by Olympus STM6 optical microscopy. 20 bonds were measured at every condition.

3. Results and discussion

3.1. Effect of bonding duration

Shear tests were performed to evaluate the bonding strength as a function of bonding duration and the results are given in Table 3. There is a trend of shear strength increases with increasing bonding duration. A slight increase of ball diameter *D* and decrease of ball height *H* are seen as the bonding duration increases.

In order to understand the underlying mechanism of bonding duration dependence of bonding strength, the interfacial structure formed with different bonding duration levels was examined by electron microscopy. Fig. 2a–c shows the overview of the interfaces with three levels of bonding duration. There is no significant difference in the interfacial structure at micro-scale, as observed by SEM at the magnification level shown in Fig. 2. In order to characterize the interfacial structure at nano-scale and verify the difference due to the variation of bonding duration, TEM analysis was performed.

A typical TEM image of the Cu–Al interface produced with a short bonding duration (level-BT1) is given in Fig. 3a which shows that only a few IMC particles are formed and they are approximately 20 nm thick. One location of the IMC particle (region A, Fig. 3a) with ordered atomic arrays was selected and the lattice image was collected (Fig. 3b). FFT analysis was consistent with CuAl₂ [0 0 1] (*Fm-3m*, *a* = 5.9988 Å) [25] joined with Al (*Fm-3m*, *a* = 4.0496 Å) [26]. In the regions where IMCs are absent, a continuous and compact layer 5–10 nm thick is situated between the copper ball and the aluminium pad (Fig. 3c). The STEM–EDX results

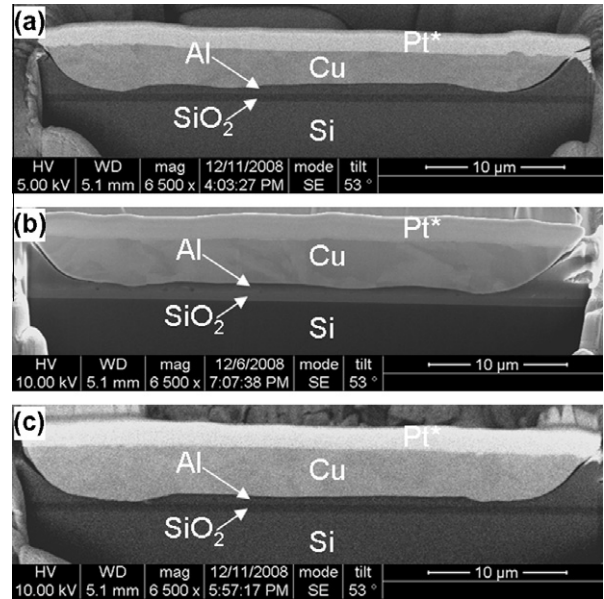


Fig. 2. SEM images showing the overview of the Cu–Al interfaces with three levels of bonding duration: (a) level-BT1; (b) level-BT2; (c) level-BT3. *A layer of Pt was deposited in order to obtain a cleaner cross section.

(Table 4) show that the main constituents of this layer are aluminium and oxygen, indicating the existence of alumina film which remains intact after bonding.

As longer bonding duration is applied, more IMCs are formed along the interface. In particular, a standard value (level-BT2) results in an almost continuous layer of IMCs (30–40 nm thick) in regions that were examined (Fig. 4a). Fig. 4b gives a higher magnification TEM image taken in region A of Fig. 4a, which presents the morphology of IMC particles. The IMC particles have a conchoidal interface linked to Al and almost linear interface with Cu, indicating the growth of those IMCs is dependent on the interdiffusion of Cu, i.e. Cu diffuse through IMCs to reacts with Al at the IMC/Al interface. STEM–EDX results (Table 4) show that the IMC is an aluminium-rich alloy. As a further confirmation, a lattice image (Fig. 4c) was collect in region A-1 of Fig. 4b and FFT is consistent with CuAl₂ [0 0 1] (*Fm-3m*, *a* = 5.9988 Å).

As proposed in our previous work [10], the initial formation of IMCs depends on the oxide rupture by ultrasonic vibration at certain pressures and temperatures. The effect of bonding duration on the removal of the oxide layer can be described by an equation developed for a contact surface pair in relative motion [27]:

$$d = t \times \frac{kvP}{H} \tag{1}$$

where *d* is the depth of material worn, *t* is time, *P* is the mean or nominal pressure, *H* is the hardness of the material, *k* is the

Table 3
Effect of bonding duration on bond dimension, shear force and shear strength.

	Level-BD1 (short duration)				Level-BD2 (standard duration)				Level-BD3 (long duration)			
	Ball diameter, μm	Ball height, μm	Shear force, gf	Shear strength, MPa	Ball diameter, μm	Ball height, μm	Shear force, gf	Shear strength, MPa	Ball diameter, μm	Ball height, μm	Shear force, gf	Shear strength, MPa
Min	37.2	12.7	12.1	–	39.5	11.6	14.1	–	40.6	10.1	15.9	–
Max	39.7	14.2	14.8	–	40.9	12.9	17.4	–	44.8	11.5	20.9	–
Mean	38.4	13.4	13.5	116.6	40.1	12.2	15.5	122.8	42.9	10.9	18.8	130.1
STDEV ^a	1.08	0.42	0.62	–	0.49	0.45	0.65	–	0.70	0.56	1.06	–

^a Standard deviation for 20 measured samples.

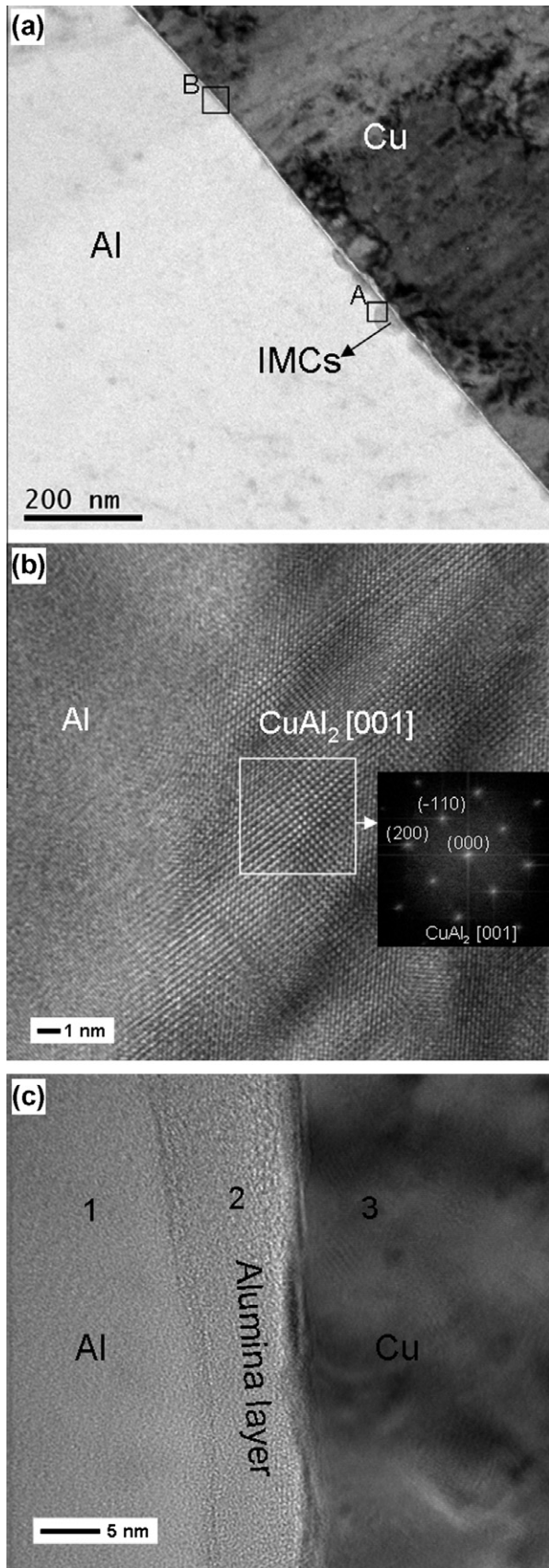


Fig. 3. (a) TEM image presenting interfacial morphology of the Cu–Al bond with a short bonding duration (level-BT1 in Table 1 for detailed bonding parameters); (b) lattice image and Fourier reconstructed pattern of region A in (a) with CuAl_2 [0 0 1] linked to the Al pad; (c) details of region B in (a) showing a 5–10 nm thick alumina layer between the copper ball and the aluminium pad.

Table 4

STEM-EDX results for regions 1–3 in Fig. 3c and 4–8 in Fig. 4b. The precision of EDX measurement of O is approximately $\pm 10\%$, and Al and Cu are approximately $\pm 2\%$.

Regions	O (K at.%)	Al (K at.%)	Cu (K at.%)
1	6	93	1
2	54	44	2
3	2	8	90
4	6	91	3
5	9	60	31
6	13	58	29
7	7	10	83
8	6	9	85

wear-coefficient constant, and v is the sliding velocity. Thereby, an increased bonding duration will lead to more sufficient removal of the oxide layer on the aluminium pad, and therefore more IMCs will be formed, resulting in a significant increase in the bonding strength. In addition, a longer interdiffusion results in thicker IMCs in Cu–Al bonds (from 20 nm for level-BT1 to 30–40 nm for level-BT2), which may also benefit to the bonding strength. However, the intermetallic phase remains the same as CuAl_2 .

3.2. Effect of substrate temperature

A slightly increased bond deformation (larger ball diameter and smaller ball height) is seen by a higher substrate temperature (Table 5). Moreover, There is an obvious trend of shear strength with an increase in substrate temperature.

At room temperature (level-ST1), the alumina occupies almost the interfacial regions (Fig. 5a), as confirmed by a high magnification TEM image (Fig. 5b) which further shows that the alumina layer is uniform and compact. The integration of the alumina acts as a barrier to interdiffusion of Cu and Al, so IMCs is unlikely to form in those regions. However, if the alumina layer is fragmented, the formation of IMCs is possible. Only a few IMC particles are formed during bonding at room temperature (Fig. 5a). Such IMCs are approximately 20 nm thick, as shown in Fig. 5c, taken from region B in Fig. 5a. As mentioned earlier, although the bonded samples were removed immediately after bonding from the work stage, they were inevitably maintained at the substrate temperature for ~ 5 s. Wire bonding at room temperature was performed with the particular aim of eliminating that post annealing. The presence of IMCs indicates that nucleation and growth of IMCs take place during bonding, although the quantity of IMCs is small at room temperature. However, A 175 °C (level-ST2, i.e. standard bonding parameters) results in an almost continuous IMC layer in regions that were examined (Fig. 4a). It is inferred that pre-heating of substrate promotes the fracture of alumina. Moreover, a pre-temperature will contribute to the actual Cu–Al interfacial temperature, accelerating interdiffusion of Cu and Al and facilitating the formation of IMCs. The formation of IMCs significantly increases the bonding strength.

According to the equilibrium phase diagram of the Cu–Al system [28], at least five intermetallic compounds – $\text{CuAl}_2(\theta)$, $\text{CuAl}(\eta_2)$, $\text{Cu}_4\text{Al}_3(\zeta_2)$, $\text{Cu}_3\text{Al}_2(\delta)$ and $\text{Cu}_9\text{Al}_4(\gamma_1)$ – possibly exist. However, only CuAl_2 is formed during bonding. Using the model of Pretorius et al. [29,30], with the effective concentration of 17 at.% Cu 83 at.% Al, the effective heats of formation for CuAl_2 , CuAl and Cu_9Al_4 are estimated to be -6.1 kJ/mol, -5.1 kJ/mol and -4.1 kJ/mol, respectively; therefore, CuAl_2 is the favoured phase to be formed. This is consistent with the results in this study that CuAl_2 nucleates during bonding, which is also in agreement with a previous TEM study by Drozdov et al. [11]. In addition, from the crystallographic point of view, the more atoms there are in a unit cell, the more difficult and less energetically favourable it is to crystallize. CuAl_2 (tetragonal, $I4/mcm$) [31,32] has 12 atoms

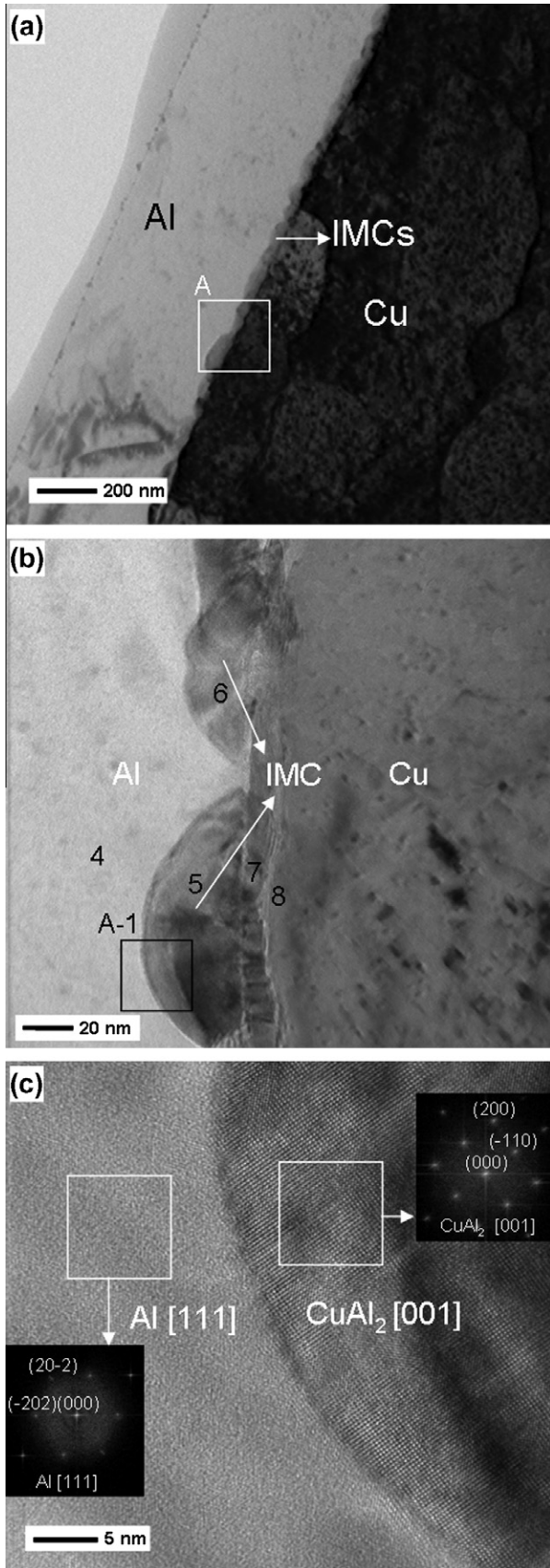


Fig. 4. (a) TEM image presenting interfacial morphology of the Cu–Al bond with a standard bonding parameters (level-BT2 in Table 1 for detailed bonding parameters); (b) details of regions A in (a) showing the morphology of IMC particles; (c) lattice image and Fourier reconstructed pattern of region A-1 in (b) with CuAl₂ [0 0 1].

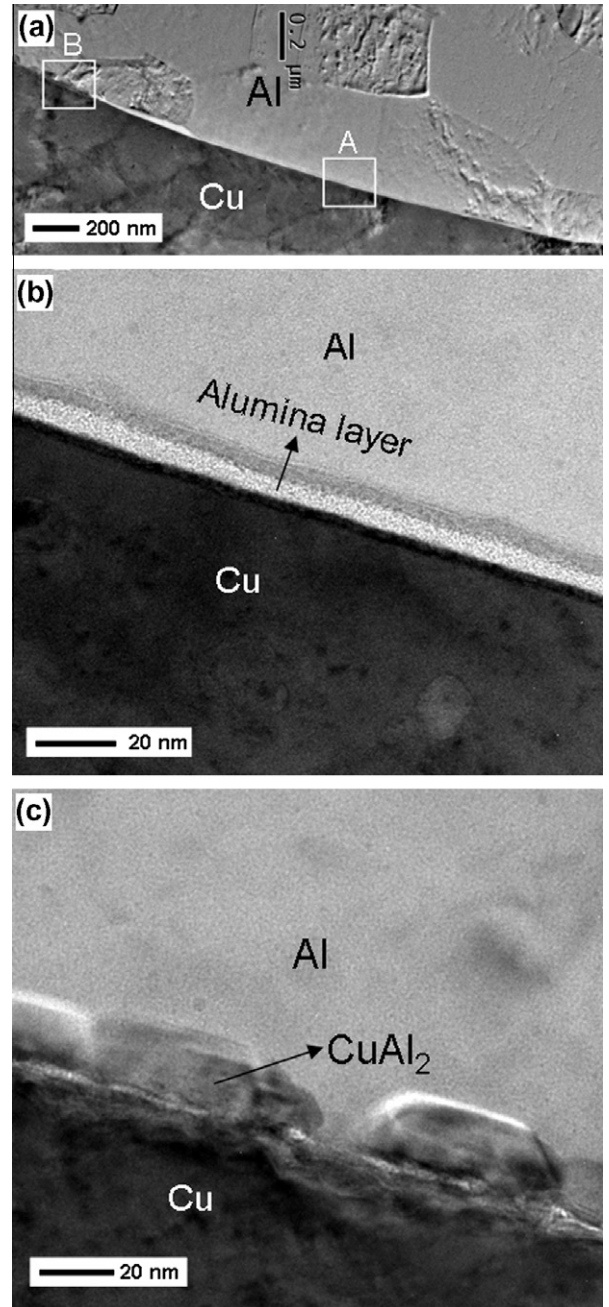


Fig. 5. (a) TEM images showing an overview of the Cu–Al interface formed at room temperature; (b) details of region A in (a) presenting a uniform layer of alumina between the copper ball and the aluminium pad; (c) details of region B in (a) presenting approximately 20-nm-thick IMC particles.

per unit cell and a short range order, and is more likely to be formed than CuAl (monoclinic, $C12/m1$, 20 atoms per unit cell) [33] and Cu₉Al₄ (cubic, $P4-3m$, 52 atoms per unit cell) [34]. Thus, it is reasonable to believe that CuAl₂ nucleates first during wire bonding. Such initial IMC layer will grow if the bonds undergo post-thermal annealing, and Cu₉Al₄ and CuAl may emerge, as has been reported that Cu₉Al₄ and/or CuAl were also formed after annealing depending on annealing conditions by electron diffraction [35] and Micro X-ray diffraction analysis [36]. In thin-film studies (where Al and Cu films were deposited one by one without breaking the vacuum) X-ray diffraction and Rutherford backscattering spectrometry found that CuAl₂ was formed initially [37,38], while elsewhere CuAl₂ and Cu₉Al₄ [39–41] reportedly grew simultaneously.

Table 5
Effect of substrate temperature on bond dimension, shear force and shear strength.

	Level-ST1 (room temperature)				Level-ST2 (175 °C)				Level-ST3 (300 °C)			
	Ball diameter, μm	Ball height, μm	Shear force, gf	Shear strength, MPa	Ball diameter, μm	Ball height, μm	Shear force, gf	Shear strength, MPa	Ball diameter, μm	Ball height, μm	Shear force, gf	Shear strength, MPa
Min	37.4	11.7	7.2	–	39.5	11.6	14.1	–	39.1	10.7	19.1	–
Max	40.9	13.5	9.5	–	40.9	12.9	17.4	–	44.5	12.1	23.9	–
Mean	39.1	12.6	8.3	69.2	40.1	12.2	15.5	122.8	42.8	11.5	21.2	147.4
STDEV ^a	0.81	0.53	0.80	–	0.49	0.45	0.65	–	0.89	0.45	1.32	–

^a Standard deviation for 20 measured samples.

4. Conclusion

The effects of bonding duration and substrate temperature on interfacial microstructure and bonding strength were investigated to establish a bonding process – microstructure – property relationship. The obtained results show that:

- (1) IMC crystallization correlates with bonding duration, as a longer duration is applied, alumina fragmentation becomes pervasive resulting in continuous alloy interfaces and therefore stronger bonds.
- (2) The interfacial structure and bonding strength are also dependent on substrate temperature. Only a few IMCs are formed during bonding at room temperature, while elsewhere there are uniform layers of alumina. Pre-heating of substrate promotes the fracture of alumina, and simultaneously contributes to the actual interfacial temperature, accelerating interdiffusion and facilitating the formation of IMCs, therefore increasing bonding strength.
- (3) The compound formed during bonding is CuAl_2 , regardless of the bonding parameters applied. The Cu–Al bonds is void-free in the as-bonded state.

Acknowledgments

This research was funded as a PMI2 Project (Grant No. RC 41) through the UK Department for Innovation, Universities and Skills (DIUS) for the benefit of the Singapore and the UK Higher Education Sectors.

References

- [1] Joshi KC. The formation of ultrasonic bonds between metals. *Weld J* 1971;50:840–8.
- [2] Mayer M, Paul O, Bolliger D, Baltes H. Integrated temperature microsensors for characterization and optimization of thermosonic ball bonding process. *IEEE Trans Compon Pack Technol* 2000;23:393–8.
- [3] Ho JR, Chen CC, Wang CH. Thin film thermal sensor for real time measurement of contact temperature during ultrasonic wire bonding process. *Sensors Actuators A: Phys* 2004;111:188–95.
- [4] Harman GG, Albers J. The ultrasonic welding mechanism as applied to aluminum-and gold-wire bonding in microelectronics. *IEEE Trans Parts Hybrids Pack* 1977;13:406–12.
- [5] Lum I, Jung JP, Zhou Y. Bonding mechanism in ultrasonic gold ball bonds on copper substrate. *Metall Mater Trans A* 2005;36:1279–86.
- [6] Lum I, Mayer M, Zhou Y. Footprint study of ultrasonic wedge-bonding with aluminum wire on copper substrate. *J Electron Mater* 2006;35:433–42.
- [7] Zhou Y, Li X, Noolu NJ. A footprint study of bond initiation in gold wire crescent bonding. *IEEE Trans Compon Pack Technol* 2005;28:810–6.
- [8] Qi J, Hung NC, Li M, Liu D. Effects of process parameters on bondability in ultrasonic ball bonding. *Scripta Mater* 2006;54:293–7.
- [9] Xu H, Liu C, Silberschmidt VV, Chen Z, Wei J. The role of bonding duration in wire bond formation: a study of footprints of thermosonic gold wire on aluminium pad. *Microelectron Int* 2010;27:11–6.
- [10] Xu H, Liu C, Silberschmidt VV, Pramana SS, White TJ, Chen Z. A re-examination of the mechanism of thermosonic copper ball bonding on aluminium metallization pads. *Scripta Mater* 2009;61:165–8.
- [11] Drozdov M, Gur G, Atzmon Z, Kaplan W. Detailed investigation of ultrasonic Al–Cu wire-bonds: I. Intermetallic formation in the as-bonded state. *J Mater Sci* 2008;43:6029–37.
- [12] Tian YH, Wang CQ, Zhou Y. Investigation of ultrasonic copper wire wedge bonding on Au/Ni plated Cu substrates at ambient temperature. *J Mater Process Technol* 2008;208:179–86.
- [13] Winchell VH, Berg HM. Enhancing ultrasonic bond development. *IEEE Trans Compon Hybrids Manuf Technol* 1978;1:211–9.
- [14] Hulst AP, Lasance C. Ultrasonic bonding of insulated wire. *Weld J* 1978;57:19–25.
- [15] Chen GKC. The role of micro-slip in ultrasonic bonding of microelectronic dimensions. *Int Hybrid Microelectron Symp* 1972;5A:111–9.
- [16] Mindlin RD. Compliance of elastic bodies in contact. *J Appl Mech* 1949;71:259–68.
- [17] Harman GG, Leedy KO. An experimental model of the microelectronic ultrasonic wire bonding mechanism. In: *Proc. 10th annual proc. reliability physics, Las Vegas, USA; 1972*. p. 49–56.
- [18] Krzanowski JE. A transmission electron microscopy study of ultrasonic wire bonding. *IEEE Trans Compon Hybrids Manuf Technol* 1990;13:176–81.
- [19] Wilson AD. Holographic interferometry applied to motion studies of ultrasonic bonders. *IEEE Trans Sonics Ultrasonics* 1971;19:453–61.
- [20] Johnson KL. One hundred years of Hertz contact. *Proc Inst Mech Eng* 1982;196:363–78.
- [21] Lum I, Huang H, Chang BH, Mayer M, Du D, Zhou Y. Effects of superimposed ultrasound on deformation of gold. *J Appl Phys* 2009;105:024905–5.
- [22] Xu H, Liu C, Silberschmidt VV, Wang H. Effects of process parameters on bondability in thermosonic copper ball bonding. In: *58th Electronic components and technology conference; 2008*. p. 1424–30.
- [23] Ding Y, Kim JK, Tong P. Effects of bonding force on contact pressure and frictional energy in wire bonding. *Microelectron Reliab* 2006;46:1101–12.
- [24] Rasband W. ImageJ Version 1.42q. Bethesda, Maryland, USA: National Institutes of Health; 2009. <<http://rsb.info.nih.gov/ij>>.
- [25] Buchler H, Range KJ. Hochdruck-Hochtemperatursynthese und kristallstruktur von $\text{Al}_{11}\text{Au}_6$ und AlAu . *J Less Common Metals* 1990;160:143–52.
- [26] Downs RT, Hall-Wallace M. The American mineralogist crystal structure database. *Am Mineral* 2003;88:247.
- [27] Peterson MB, Winer WO. *Wear control handbook*. New York: ASME; 1980.
- [28] Murray JL. The aluminum–copper system. *Int Metals Rev* 1985;30:211–33.
- [29] Pretorius R, Theron CC, Vantomme AC, Mayer JC. Compound phase formation in thin film structures. *Crit Rev Solid State Mater Sci* 1999;24:1–62.
- [30] Pretorius R, Vredenberg AM, Saris FW, de Reus R. Prediction of phase formation sequence and phase stability in binary metal–aluminum thin-film systems using the effective heat of formation rule. *J Appl Phys* 1991;70:3636–46.
- [31] Meetsma A, de Boer JL, van Smaalen S. Refinement of the crystal structure of tetragonal Al_2Cu . *J Solid State Chem* 1989;83:370–2.
- [32] Owen EA, Preston GD. X-ray analysis of solid solutions. *Proc Phys Soc* 1924;36:14–30.
- [33] El-Boragy M, Szepan R, Schubert K. Crystal structure of $\text{Cu}_3\text{Al}_2 + (\text{h})$ and $\text{CuAl}(\text{r})$. *J Less Common Metals* 1972;29:133–40.
- [34] Arnberg L, Westman S. Refinement and test of twinning of the $\gamma\text{-Cu}_9\text{Al}_4$ structure. *Acta Crystallogr A* 1978;34:399–404.
- [35] Drozdov M, Gur G, Atzmon Z, Kaplan W. Detailed investigation of ultrasonic Al–Cu wire-bonds: II. Microstructural evolution during annealing. *J Mater Sci* 2008;43:6038–48.
- [36] Kim HJ, Lee JY, Paik KW, Koh KW, Won JH, Choe SY, et al. Effects of Cu/Al intermetallic compound (IMC) on copper wire and aluminum pad bondability. *IEEE Trans Compon Pack Technol* 2003;26:367–74.
- [37] Gershinskii AE, Fomin BI, Cherepov EI, Edelman FL. Investigation of diffusion in the Cu–Al thin film system. *Thin Solid Films* 1977;42:269–75.
- [38] Tamou Y, Li J, Russell SW, Mayer JW. Thermal and ion beam induced thin film reactions in Cu–Al bilayers. *Nucl Instrum Methods Phys Res Section B* 1992;64:130–3.
- [39] Campisano SU, Costanzo E, Scaccianoce F, Cristofolini R. Growth kinetics of θ -phase in Al–Cu thin-film bilayers. *Thin Solid Films* 1978;52:97–101.
- [40] Rajan K, Wallach ER. A transmission electron microscopy study of intermetallic formation in aluminium–copper thin-film couples. *J Cryst Growth* 1980;49:297–302.
- [41] Hamm RA, Vandenberg JM. A study of the initial growth kinetics of the copper–aluminum thin-film interface reaction by in situ X-ray diffraction and Rutherford backscattering analysis. *J Appl Phys* 1984;56:293–9.